Journal of Power and Energy Engineering, 2021, 9, 19-40
https://www.scirp.org/journal/jpee
ISSN Online: 2327-5901
ISSN Print: 2327-588X

Exergoeconomic Evaluation and Optimization of Dual Pressure Organic Rankine Cycle (ORC) for Geothermal Heat Source Utilization

Dodeye Igbong[1], Oku Nyong[1*], James Enyia[1], Benjamin Oluwadare[2], Mafel Obhua[3]

[1]Department of Mechanical Engineering, Cross River University of Technology, Calabar, Nigeria
[2]Department of Mechanical Engineering, Ekiti State University, Ado Ekiti, Nigeria
[3]Nigeria Maritime University, Okerenkok, Nigeria
Email: *nyong.oku@gmail.com

How to cite this paper: Igbong, D., Nyong, O., Enyia, J., Oluwadare, B. and Obhua, M. (2021) Exergoeconomic Evaluation and Optimization of Dual Pressure Organic Rankine Cycle (ORC) for Geothermal Heat Source Utilization. *Journal of Power and Energy Engineering*, **9**, 19-40.
https://doi.org/10.4236/jpee.2021.99002

Received: June 16, 2021
Accepted: September 27, 2021
Published: September 30, 2021

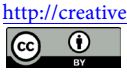

Abstract

In the present study, a dual-pressure organic Rankine cycle (DORC) driven by geothermal hot water for electricity production is developed, investigated and optimized from the energy, exergy and exergoeconomic viewpoint. A parametric study is conducted to determine the effect of high-stage pressure P_{HP} and low-stage pressure P_{LP} variation on the system thermodynamic and exergoeconomic performance. The DORC is further optimized to obtain maximum exergy efficiency optimized design (EEOD case) and minimum product cost optimized design (PCOD case). The exergy efficiency and unit cost of power produced for the optimization of EEOD case and PCOD case are 33.03% and 3.059 cent/kWh, which are 0.3% and 17.4% improvement over base case, respectively. The PCOD case proved to be the best, with respect to minimum unit cost of power produced and net power output over the base case and EEOD case.

Keywords

Geothermal Water, Dual Pressure Organic Rankine Cycle, Exergoeconomic Factor, Optimization

1. Introduction

In recent years, the utilization of low-grade heat sources such as geothermal, biomass, solar and power and industrial process waste heat, are becoming more and more attractive as a sustainable approach towards ameliorating environmental issues, such as air pollution, acid rain, global warming and ozone layer

depletion caused by greenhouse gas emission from fossil fuel combustion. It is also considered a potential solution to reducing the energy shortage being experienced due to the rapid growth in population and economic activities around the world. Organic Rankine cycle (ORC) is widely used and considered a promising heat-to-power conversion technology that uses lower boiling temperature working fluids, which makes it suitable, flexible and efficient for converting a wide range of heat source temperature to useful power output [1] [2] [3] [4]. It has the advantage of small plant size and modularity, easy construction and low cost of operation [4]. It also has capability for better temperature matching characteristics between working fluids and the low-grade heat source fluid, especially for advance ORC configuration, thus minimizing exergy loss in the evaporators while increasing cycle exergy efficiency [3] [5].

Geothermal energy is a low-medium grade heat source, which is attracting growing attention for power generation due to concern about environmental pollution problems from fossil fuel consumption. The advantage of geothermal energy over other renewable energy like wind and solar energies, is that its availability is all year round and, independent of time of day or seasons. The utilization of geothermal energy is increasing worldwide, in 2016 the total install generating capacity was 12.7 GW with annual electricity generation of 80.9 terawatt-hour (TWh) in 2015, accounting for 3% global electricity production [6]. Although it represents a small percentage of electricity production worldwide, in some countries geothermal accounts for more than 10% of the national electricity generation capacity [7]. At present, electricity generation from geothermal resources uses three major type of power plants: the dry-steam plants, flash plants (single, double or triple), or binary plants, depending on the state of the fluid and its temperature [7]. For geothermal wells producing high temperature steam (>235˚C), dry-steam plants are used. When the steam temperature is >180˚C and <235˚C, the flash plants are more suitable, and lastly the binary plants are used for hydrothermal well that produces water temperature <180˚C. In binary cycle, the working fluid other than the geothermal water undergoes a closed cycle, where it evaporates at the heat exchanger, expands in the turbine, condenses in the condenser and it is pumped back to the heat exchanger. Binary plants are often based on ORC or Kalina cycles, whereas the Kalina cycle uses working fluid mixture of water and ammonia (NH_3H_2O) which produces two vapour-components at variable temperature, the ORC uses pure organic working fluids with specific evaporation temperature and better matching characteristic with the geothermal fluid, therefore resulting in higher thermodynamic and exergy efficiencies.

Several Scholars have conducted studies on suitable technology options for low-grade heat source utilization such as geothermal, in which ORC is considered the best technology for heat recovery, with cycle modification capable of achieving higher performance [2] [5] [8] [9]. The dual-pressure organic Rankine cycle (DORC) consists of two evaporation processes with different pressure val-

ues and a condensation process. This can reduce the heat transfer temperature difference between the working fluids and the heat source fluid, significantly decreasing the exergy destruction in the evaporator [2] [3]. Several studies have reported on the performance advantage of the DORC system to the conventional single organic Rankine cycle (SORC). Li *et al*. [10] investigated the thermodynamic performance of series two-stage ORC (STORC), parallel two-stage ORC (PTORC) and single-pressure ORC (SORC) systems using 90˚C - 120˚C geothermal water and R245fa. Results showed an increase in the net power output for the STORC and PTORC compared with the SORC system. Shokati *et al*. [11] conducted an energy, exergy and exergoeconomic comparative investigation on the SORC, DORC, dual-loop ORC and the Kalina cycle based on heat source temperature of 175˚C. Results showed that the net power output of DORC was 15.2% higher than the SORC, 35.1% higher than dual-loop ORC, and 43.5% higher than the Kalina cycle system. Thierry *et al*. [12] investigated the performance of DOC using working fluid mixture for heat source temperature range of 90˚C - 110˚C. Results indicate that DORC efficiency increased by 12.4% relative to the SORC system. Manente *et al*. [13] investigated and compared the thermodynamic performance of the SORC and DORC systems driven by geothermal heat source of 100˚C - 200˚C temperature range. Results showed DORC gave better performance than SORC, with performance gain of DORC diminishing as heat source temperature increased. Sadeghi *et al*. [14] evaluated and compared the performance of SORC, STORC and PTORC using zeotropic working fluids and driven by geothermal heatsource temperature of 100˚C. Results showed a 34.3% net power output increase for STORC relative to the SORC system. Li *et al*. [15] studied the thermoeconomic performance of ORC with separate and induction turbine layouts, and analyzed the effect of the low-stage and high-stage pressures on the thermoeconomic performance of the system. Results showed that the induction turbine produced better net power output, with significant decrease in the specific investment cost.

There exist in public domain several researches comparing performance of different ORC layouts and system optimization of the DORC. However, a few studies have investigated the exergoeconomic performance of the DORC system with optimization towards optimal system exergy efficiency and minimum product total cost design. Even though DORC systems produces better performance compared with the conventional SORC, their much higher specific investment cost due to their complex configurations consisting of two evaporation processes, two turbine expansion processes and two pumping processes, might be a drawback. Therefore, it is essential to investigate the thermoeconomic and exergoeconomic performance of DORC applications.

The present study, investigates the exergoeconomic optimization of dual-pressure ORC using geothermal heat source. Thermodynamic and thermoeconomic analysis was performed to determine the system first and second law efficiencies, as well as the exergy unit cost rate for each stream. Parametric analysis was also

conducted to determine the influence of the high-stage and low-stage pressures, working fluids mass flow and heat source temperature on the system overall exergy efficiency and product unit cost. In addition, optimization was performed to obtain optimal decision parameters to attain maximum exergy efficiency optimized design (EEOS case) and minimum product cost optimized design (PCOD case). Finally, to design a cost-efficient system the exergoeconomic parameters like the exergoeconomic factor and cost of exergy destruction were determined for each component in order to identify potential opportunities for system improvement.

2. System Description

Figure 1 shows the schematic diagram of the dual-pressure organic Rankine cycle (DORC) driven by geothermal hot water. The ORC system consist of a superheater, the high pressure (HP) and low pressure (LP) evaporators, HP and LP preheaters, HP and LP turbines, an isobaric condenser and the PH and LP pumps. The LP pump compresses the organic working fluid (state 1) exiting the condenser, the pressurize fluid (state 2) then flows through the preheater 1 where heat from the LP evaporator exit stream is used to increase the fluid enthalpy. The working fluid leaving the preheater is divided into two streams. One part of the organic working fluid flows to the LP evaporator (state 3a) and the other part moves to the HP pump (state 3b) where it is further compressed to

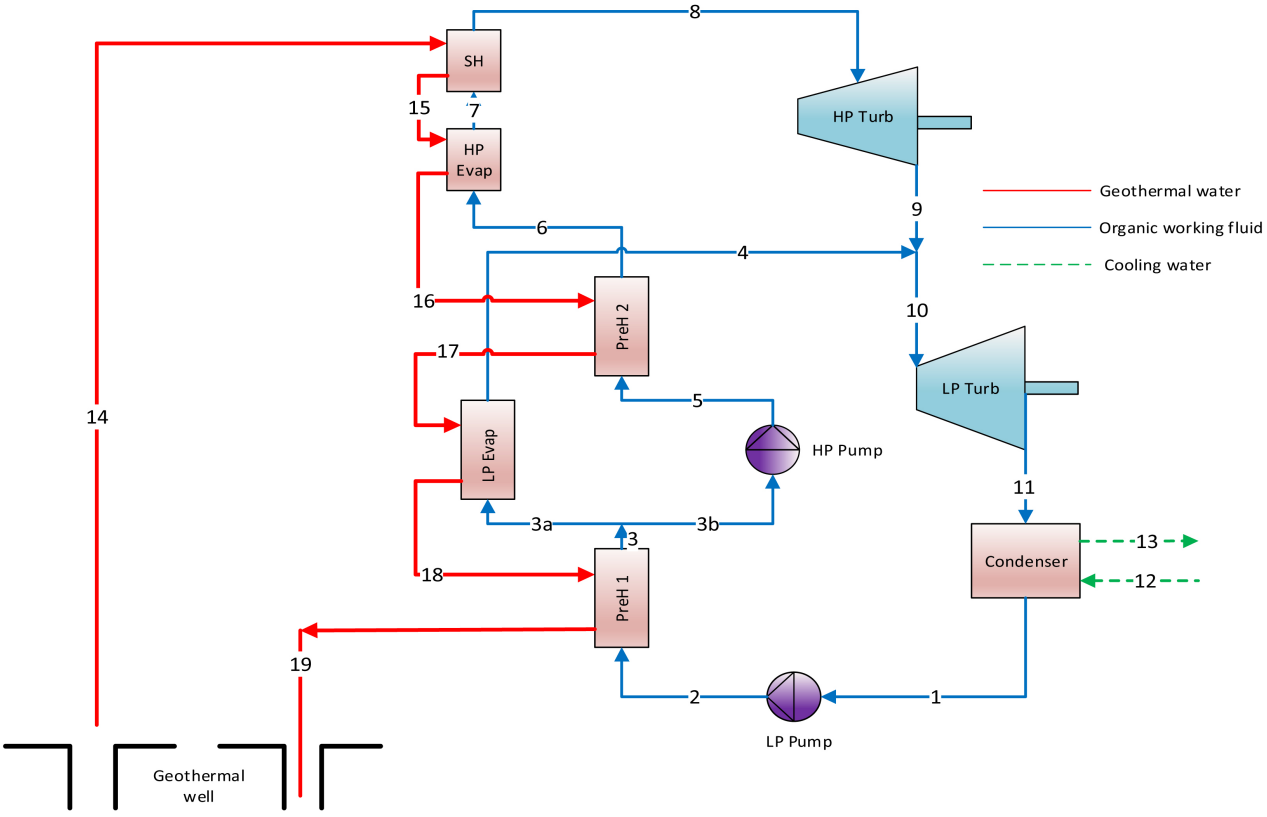

Figure 1. Schematic diagram of dual pressure ORC driven by geothermal heat source.

high-stage pressure. The compressed fluid from the HP pump (state 5) flows through the preheater 2, absorbing heat before entering the HP evaporator (state 6). The vaporized fluid (state 7) is then superheated before exiting the superheater (state 8) to undergo expansion in the HP turbine. The working fluid leaving the HP turbine (state 9) mixes with the fluid stream from the LP evaporator (state 4) and then flows to the LP turbine inlet (state 10) where it undergoes second turbine expansion. The LP turbine exhaust vapour (state 11) is condensed in the condenser into liquid (state 1) by the cooling water entering (state 12) and leaving (state 13) the condenser. The liquid working fluid (state 1) is then pumped to the preheater 1 and the entire cycle is completed. The geothermal hot water is the heat source that have been used to drive the ORC system. It is a medium-temperature heat source with maximum temperature of 150˚C at 2525 kPa pressure.

The geothermal resource from the geothermal well (state 14) enters the superheater and exits (state 15) into the HP evaporator where the working fluid is superheated and vaporize, respectively. The hot water streams from HP evaporator (state 16) preheats the high pressure (HP) working fluid in the Preheater 2, then leaves to vaporize (state 17) the low pressure (LP) working fluid. The remaining enthalpy in the hot water leaving (state 18) the LP evaporator is used to preheat the working fluid in preheater 1, and finally delivered back to the geothermal well (state 19). It is worth noting that, the working fluid pressure leaving the LP evaporator (state 4) is equal to the HP turbine exhaust vapour pressure (state 9).

3. Thermodynamic Analysis

For the purpose of system analysis, each component of the DORC is considered a control volume in which mass and energy conservation principles, as well as the second law of thermodynamics are applied. The EES software developed by Ibrahim and Klein [16] have been employed to model all processes in the ORC system.

The following simplified assumptions are further employed in modelling of the ORC:

- The ORC system operates at steady-state condition.
- Pressure drops in all heat exchangers and pipes are negligible.
- Dry and isentropic working fluid at the turbine inlets are superheated vapor.
- Pinch point temperature difference at the heat exchanger is 10˚C.
- Changes in potential and kinetic are negligible.

The mass and energy conservation, as well as exergy balance relations for each system component are represented as [17]:

$$\sum \dot{m}_{in} = \sum \dot{m}_{out} \tag{1}$$

$$\sum \dot{m}_{in} h_{in} + \dot{Q}_{cv} - \sum \dot{m}_{out} h_{out} - \dot{W}_{cv} = 0 \tag{2}$$

$$\sum \dot{E}_{in} - \sum \dot{E}_{out} + \sum \dot{E}_{heat} + \sum \dot{W}_{J} - \dot{E}_{D,J} = 0 \tag{3}$$

Neglecting the potential and kinetic exergies, the total exergy ($\dot{E}$) is considered as the sum of the physical and chemical components expressed as [17]:

$$\dot{E} = \dot{E}_{ph} + \dot{E}_{ch} \tag{4}$$

The physical exergy quantifies the maximum obtainable useful work when the system state changes due to variation in pressure and temperature from the specific state (T, P) to reference state (T_0, P_0). The specific physical and chemical exergies are expressed as follow:

$$\dot{E}_{ph} = \dot{m}\left[\left(h - h_0\right) - T_0\left(s - s_0\right)\right] \tag{5}$$

$$\dot{E}_{ch} = \dot{m}\left[\sum_{i=1}^{n} X_i ex_{ch,i} + RT_0 \sum_{i=1}^{n} X_i Ln\left(X_i\right)\right] \tag{6}$$

In the exergy analysis of a system, the product exergy ($\dot{E}_p$) and fuel exergy ($\dot{E}_f$) of both the system components and the entire system are calculated separately. For each system component the exergy destruction is defined as the difference between the product and fuel exergies:

$$\dot{E}_{D,J} = \dot{E}_{f,J} + \dot{E}_{p,J} \tag{7}$$

The ORC performance evaluates the system energy utilization factor, defined in terms of the thermal efficiency and exergy efficiency.

Thermal efficiency is the ratio of the net power output to the input energy from the geothermal heat source [2]:

$$\eta_{thermal} = W_{net} / Q_{in} \tag{8}$$

where,

$$\dot{W}_{net} = \dot{W}_{HP\_turb} + \dot{W}_{LP\_turb} - \dot{W}_{pump1} - \dot{W}_{pump2} \tag{9}$$

$$\dot{Q}_{in} = \dot{m}_{14}\left(h_{14} - h_{19}\right) \tag{10}$$

The exergy efficiency is expressed as follows

$$\eta_{exergy} = \left(W_{net} + E_{ref}\right) / \dot{E}_{in} \tag{11}$$

where,

$$\dot{E}_{in} = \dot{E}_{14} - \dot{E}_{19} \tag{12}$$

The overall system efficiency, η_{sys}, and the heat recovery effectiveness, ϕ, of the ORC are calculated as follows:

$$\eta_{sys} = Q_{in} / \dot{m}_{14}\left(h_{14} - h_0\right) \tag{13}$$

$$\phi = W_{net} / \dot{m}_{14}\left(h_{14} - h_0\right) \tag{14}$$

where, h_0 is specific heat enthalpy of heat source water at ambient temperature.

The energy and exergy relations for each component of the ORC system is shown in **Table 1**.

4. Exergoeconomic Analysis

Exergoeconomic analysis is an approach that combines exergy and economic analyses in order to facilitate better design and more cost-efficient systems. The

Table 1. Energy and exergy equations for the ORC.

Components	Organic Rankine Cycle	
	Energy equations	**Exergy equation**
Pump 1	$\eta_{Pump1} = \frac{w_s}{w_A} = \frac{h_{2s} - h_1}{h_2 - h_1}$ $W_{Pump1} = \dot{m}_1 (h_2 - h_1)$	$\dot{E}_1 + \dot{W}_{pump1} - \dot{E}_2 = \dot{E}_{Destruction}$
Pump 2	$\eta_{Pump2} = \frac{w_s}{w_A} = \frac{h_{5s} - h_{3b}}{h_5 - h_{3b}}$ $W_{Pump2} = \dot{m}_5 (h_5 - h_{3b})$	$\dot{E}_{3b} + \dot{W}_{pump2} - \dot{E}_5 = \dot{E}_{Destruction}$
Condenser	$\dot{m}_{cooling} (h_{13} - h_{12}) = \dot{m}_{11} (h_{11} - h_1)$ $\dot{Q}_{Econ} = \dot{m}_{11} (h_{11} - h_1)$	$\dot{E}_{11} + \dot{E}_{12} - \dot{E}_1 - \dot{E}_{13} = \dot{E}_{Destruction}$
Superheater	$\dot{m}_{14} (h_{14} - h_{15}) = \dot{m}_8 (h_8 - h_7)$ $\dot{Q}_{SuperH} = \dot{m}_8 (h_8 - h_7)$	$\dot{E}_{14} + \dot{E}_7 - \dot{E}_{15} - \dot{E}_8 = \dot{E}_{Destruction}$
HP Evaporator	$\dot{m}_{15} (h_{15} - h_{16}) = \dot{m}_6 (h_7 - h_6)$ $\dot{Q}_{HP\_Evap} = \dot{m}_6 (h_7 - h_6)$	$\dot{E}_{15} + \dot{E}_6 - \dot{E}_7 - \dot{E}_{16} = \dot{E}_{Destruction}$
HP Turbine	$\eta_{HP\_turb} = \frac{w_A}{w_s} = \frac{h_8 - h_9}{h_8 - h_{9s}}$ $W_{HP\_turb} = \dot{m}_8 (h_8 - h_9)$	$\dot{E}_8 - \dot{W}_{HP\_turb} - \dot{E}_9 = \dot{E}_{Destruction}$
Preheater 1	$\dot{m}_{18} (h_{18} - h_{19}) = \dot{m}_3 (h_3 - h_2)$ $\dot{Q}_{preH1} = \dot{m}_3 (h_3 - h_2)$	$\dot{E}_{18} + \dot{E}_2 - \dot{E}_{19} - \dot{E}_3 = \dot{E}_{Destruction}$
LP Evaporator	$\dot{m}_{17} (h_{17} - h_{18}) = \dot{m}_4 (h_4 - h_{3a})$ $\dot{Q}_{LP\_Evap} = \dot{m}_4 (h_4 - h_{3a})$	$\dot{E}_{17} + \dot{E}_{3a} - \dot{E}_{18} - \dot{E}_4 = \dot{E}_{Destruction}$
LP Turbine	$\eta_{LP\_turb} = \frac{w_A}{w_s} = \frac{h_{10} - h_{11}}{h_{10} - h_{11s}}$ $W_{LP\_turb} = \dot{m}_{10} (h_{10} - h_{11})$	$\dot{E}_{10} - \dot{W}_{LP\_turb} - \dot{E}_{11} = \dot{E}_{Destruction}$
Preheater 2	$\dot{m}_{16} (h_{16} - h_{17}) = \dot{m}_5 (h_6 - h_5)$ $\dot{Q}_{preH2} = \dot{m}_5 (h_6 - h_5)$	$\dot{E}_{16} + \dot{E}_5 - \dot{E}_{17} - \dot{E}_6 = \dot{E}_{Destruction}$

analysis provides information about the cost formation process and cost of unit exergy of each stream. This analysis is conducted through the formation of cost balance equations and auxiliary equations for each component expressed in the form [11]:

$$\sum \dot{C}_{i,J} + \dot{C}_{q,J} + \dot{Z}_J = \sum \dot{C}_{e,J} + \dot{C}_{w,J} \tag{15}$$

where,

$$\dot{C} = c\dot{E} \tag{16}$$

In the equations above, $\dot{C}$ is the cost rate of exergy (\$/hr) and c is the cost of unit exergy of each stream (\$/GJ). Also, C_q and C_w represent the heat transfer rate of each component and the work associated costs, respectively.

The cost balance equation for the entire system is usually formulated as follow [17]:

$$\dot{C}_{P,total} = \dot{C}_{f,total} + \dot{Z}_{total} \tag{17}$$

where, $\dot{C}_P$ denotes total product related costs, $\dot{C}_f$ is the fuel cost rate and $\dot{Z}$ is the total costs related to capital investment and operation and maintenance.

The Investment cost rate ($\dot{Z}_J$) of J^{th} component is defined as the sum of the capital investment ($\dot{Z}_J^{CI}$) and operation and maintenance costs ($\dot{Z}_J^{OM}$).

$$\dot{Z}_J = \dot{Z}_J^{CI} + \dot{Z}_J^{OM} \tag{18}$$

The annual levelized capital investment cost is computed as [17]:

$$\dot{Z}_J = (CRF/\tau) Z_J + (y_J/\tau) Z_J + \omega_J \dot{E}_{P,J} + R_J/\tau \tag{19}$$

where Z_J is the capital cost for J component, and is calculated with relations as expressed in **Appendix A**. *CRF* denotes the capital recovery factor given as:

$$CRF = i_r (1+i_r)^n \Big/ \left((1+i_r)^n - 1\right) \tag{20}$$

where, i_r is the interest rate, and n is the number of useful years the plant is in operation.

In Equation (19), τ is the annual hours of plant operation, y_J is the fixed cost and ω_J is the variable cost relating to operation and maintenance.

The term R_J refers to all other costs independent from investment cost and operation and maintenance costs. The first term in Equation (19) is much larger than the two last terms, therefore the two last terms can be neglected.

Table 2 shows the cost balance and auxiliary cost equations for each component

Table 2. Component cost balance and auxiliary cost equation of the ORC.

Components	Organic Rankine cycle	
	Cost equations	**Auxiliary equation**
Pump 1	$\dot{C}_1 + \dot{C}_{w,pump1} + \dot{Z}_{pump1} = \dot{C}_2$	
Condenser	$\dot{C}_{11} + \dot{C}_{12} + \dot{Z}_{cond} = \dot{C}_1 + \dot{C}_{13}$	$c_{11} = c_1$; $c_{12} = 0$
Preheater 1	$\dot{C}_2 + \dot{C}_{18} + \dot{Z}_{preH1} = \dot{C}_3 + \dot{C}_{19}$	$c_2 = c_3$; $c_{3a} = c_3$
LP Turbine	$\dot{C}_{10} + \dot{Z}_{LP\_turb} = \dot{C}_{11} + \dot{C}_{w,LP\_turb}$	$c_{11} = c_{10}$ $c_{w,LP\_turb} = c_{w,pump1}$
LP Evaporator	$\dot{C}_{3a} + \dot{C}_{17} + \dot{Z}_{LP\_evap} = \dot{C}_4 + \dot{C}_{18}$	$c_{3a} = c_4$; $c_{3a} = c_{3b}$
Preheater 2	$\dot{C}_5 + \dot{C}_{16} + \dot{Z}_{preH2} = \dot{C}_6 + \dot{C}_{17}$	$c_5 = c_6$
Pump 2	$\dot{C}_{3b} + \dot{C}_{w,pump2} + \dot{Z}_{pump2} = \dot{C}_5$	$\dot{C}_{w,pump2} = \dot{C}_{w,pump2}$
HP Turbine	$\dot{C}_8 + \dot{Z}_{HP\_turb} = \dot{C}_9 + \dot{C}_{w,HP\_turb}$	$c_9 = c_8$; $c_{w,HP\_turb} = c_{w,pump2}$
HP Evaporator	$\dot{C}_6 + \dot{C}_{15} + \dot{Z}_{HP\_evap} = \dot{C}_7 + \dot{C}_{16}$	$c_6 = c_7$
Superheater	$\dot{C}_7 + \dot{C}_{14} + \dot{Z}_{SuperH} = \dot{C}_8 + \dot{C}_{15}$	$c_7 = c_8$
Mixer	$\dot{C}_4 + \dot{C}_9 + \dot{Z}_{mixer} = \dot{C}_{10}$	
Separator	$\dot{C}_3 = \dot{C}_{3a} + \dot{C}_{3b}$	$c_{3a} = c_{3b}$

of the ORC system.

Exergoeconomic Factors

The exergoeconomic factor (f_J), and the cost of exergy destruction are very important exergoeconomic parameters that are used for evaluating the economic performance of the entire system and each component.

- **Exergoeconomic factor (f_J):**

Exergoeconomic factor (f_J) defines the proportion of capital investment and operation and maintenance costs in the exergy destruction and exergy loss related costs for each component [11] [17].

$$f_J = \dot{Z}_J \Big/ \left[\dot{Z}_J + \left(\dot{C}_{D,J} + \dot{C}_{L,J} \right) \right] \tag{21}$$

- **Cost of exergy destruction:**

The cost of exergy destruction is often referred to as a hidden cost, as it does not appear in the cost balance equation of the components. The cost of exergy destruction, cost of product and cost of fuel can be expressed as follows [18]:

$$\dot{C}_{D,J} = c_{f,J} \dot{E}_{D,J} \tag{22}$$

$$\dot{C}_{P,J} = c_{p,J} \dot{E}_{P,J} \tag{23}$$

$$\dot{C}_{F,J} = c_{f,J} \dot{E}_{F,J} \tag{24}$$

where c_f and c_p denotes average cost per unit fuel and the cost per unit product for each component.

5. Model Verification

The thermodynamic model developed for the DORC system being investigated is first validated against available public literature [20]. A comparison of the results obtained in present work with those reported in Manente *et al.* [20] is shown in **Table 3**. It is observed that there is a good agreement between results obtained from present study and those reported in literature.

The Input data and assumptions made for the parametric study of the DORC system is listed in **Table 4**.

5.1. Results and Discussion

The thermodynamic properties, exergy rate $\dot{E}$, exergy cost rate $\dot{C}$ [$/hr] and cost rate of unit exergy c[$/GJ] at each stream for the developed model of the DORC system based on the input conditions listed in **Table 4** is presented in **Table 5**. It can be observed that the cost per unit exergy for the superheater, evaporators and preheaters have the highest values. This is due to the high heat losses experienced in these components. **Table 6** presents a summary of the exergy of fuel (*i.e.* input exergy) $\dot{E}_f$, exergy of product $\dot{E}_p$, exergy destruction rate $\dot{E}_D$, and exegetic efficiency ε, of individual components of the DORC base case. The condenser has the highest value of exergy destruction rate compared to other components, and with a corresponding component exegetic

Table 3. Comparison of the results from present models with those reported in [19].

Parameters	Working fluid-Isobutane		
	Present Work	Manente *et al.* [19]	Relative error [%]
T_{Sat_HP} [˚C]	113.40	113.30	+0.088
T_{Sat_LP} [˚C]	76.57	76.60	−0.039
P_{HP} [KPa]	2525	2530	−0.198
P_{LP} [KPa]	1230	1230	0.0
$\dot{m}_{HP}$ [Kg/s]	62.90	62.90	0.0
$\dot{m}_{LP}$ [Kg/s]	32.74	32.80	−0.183
η_{th} [%]	10.59	10.22	+3.493
η_{sys} [%]	7.026	7.066	−0.569
W_{net} [KW]	3859	3871	−0.310

Table 4. The DORC system input data.

Parameters	Values
Ambient Temperature, T_{amb}	20 [˚C]
Ambient Pressure, P_{amb}	101 [kPa]
Geothermal Water Temperature, T_{14}	150 [˚C]
Geothermal Water Pressure, P_{14}	2525 [kPa]
Geothermal water mass flow rate, $\dot{m}_{14}$	45 [Kg/s]
Pinch point temperature difference in the evaporator, ΔT_{Evap}	10 [˚C]
Cooling water entry temperature, T_{12}	25 [˚C]
Condensation temperature, T_{cond}	29 [˚C]
Pinch point temperature difference in the condenser, ΔT_{cond}	10 [˚C]
Turbine efficiency, η_{turb}	85 [%]
Pump efficiency, η_{pump}	70 [%]
Annual operating hours, τ	8000 [hr./year]
Interest rate, i_r	15 [%]
Plant years of operation, n	20 years

efficiency of 99.87%.

After the condenser, the next components with significant contribution to the cycle exergy destruction rate are the HP evaporator, LP turbine and preheater 1, with exergy efficiencies of 99.91%, 98.92% and 99.98%, respectively.

The DORC base case exergoeconomic parameters are presented in **Table 7**. From exergoeconomic analysis viewpoint, components with the highest value of $\dot{Z}+\dot{C}_D$ should be treated with higher impotence in terms of implementing component improvement effort. Therefore, the LP turbine is of higher importance from exergoeconomic viewpoint. The high value of f indicates that the HP evaporator cost rates associated with capital investment cost dominates the contribution associated with exergy destruction in the LP turbine. To reduce the value of $\dot{Z}+\dot{C}_D$ for the LP turbine, capital investment cost should be reduce by

Table 5. Thermodynamic flow parameters, exergy flow rates, cost flow rates and unit cost of exergy for Isobutane.

State	Working Fluid	T [˚C]	P [KPa]	$\dot{m}$ [Kg/s]	$\dot{E}_{ex}$ [MW]	$\dot{C}$ [$/h]	c [$/GJ]
1	Isobutane	39.00	517	43.34	8.238	154.40	5.205
2	Isobutane	39.67	1250	43.34	8.322	161.40	5.389
3	Isobutane	76.57	1250	43.34	12.371	188.30	4.229
4	Isobutane	76.57	1250	14.48	7.658	86.42	3.135
5	Isobutane	78.19	2525	28.87	8.347	135.70	4.517
6	Isobutane	113.3	2525	28.87	11.407	158.10	3.850
7	Isobutane	113.3	2525	28.87	16.176	190.00	3.263
8	Isobutane	114.3	2525	28.87	16.278	194.50	3.319
9	Isobutane	82.45	1250	28.87	15.646	186.90	3.319
10	Isobutane	80.48	1250	43.34	23.303	436.70	5.205
11	Isobutane	52.42	517	43.34	21.979	411.90	5.205
12	Water	25.00	101	877.30	17.108	0	0
13	Water	29.00	101	877.30	30.809	264.60	2.386
14	Water	150.00	2525	45.00	23.345	115.40	1.373
15	Water	149.40	2525	45.00	23.243	114.90	1.373
16	Water	123.30	2525	45.00	18.460	91.24	1.373
17	Water	106.30	2525	45.00	15.391	76.07	1.373
18	Water	86.57	2525	45.00	11.854	58.59	1.373
19	Water	63.69	2525	45.00	7.792	38.51	1.373

Table 6. Results of exergy analysis of the DORC system components.

Components	Exergy Parameters			
	$\dot{E}_p$ [KW]	$\dot{E}_f$ [KPa]	$\dot{E}_D$ [KW]	ε [%]
HP Turbine	626.1[a]	632.4	6.229	99.02
LP Turbine	1310.0	1325.0	14.270	98.92
Condenser	30,809.0	30,849.0	39.110	99.87
LP Pump 1	8322.0	8323.0	1.637	99.98
Preheater 1	12,371.0	12,384.0	12.59	99.90
LP Evaporator	7658.0	7669.0	11.470	99.85
HP Pump 2	8347.0	8349.0	1.884	99.98
Preheater 2	11,407.0	11,416.0	8.323	99.93
HP Evaporator	16,176.0	16,191.0	14.640	99.91
Superheater	16,278.0	16,279.0	0.4564	100.00

Table 7. Results of exergoeconomic parameters of the DORC system components.

Components	Exergoeconomic Parameters					
	c_p [$/GJ]	c_f [$/GJ]	$\dot{C}_D$ [$/hr]	$\dot{Z}_J$ [$/hr]	$\dot{Z}_J+\dot{C}_{D,J}$ [$/hr]	f [%]
HP Turbine	9.979	3.319	0.07441	14.940	15.010	99.50
LP Turbine	9.979	5.205	0.26730	22.250	22.520	98.81
Condenser	2.386	2.319	0.32640	7.139	7.465	95.63
LP Pump 1	5.389	5.254	0.03096	4.003	4.034	99.23
Preheater 1	4.229	4.072	0.18450	6.831	7.016	97.37
LP Evaporator	3.135	2.912	0.12020	6.024	6.144	98.04
HP Pump 2	4.517	4.305	0.02919	6.349	6.378	99.54
Preheater 2	3.850	3.672	0.11000	7.208	7.318	98.50
HP Evaporator	3.263	3.118	0.16440	8.240	8.404	98.04
Superheater	3.319	3.251	0.00534	3.968	3.968	99.87

using cheaper turbine. The next components with the highest $\dot{Z}+\dot{C}_D$ value are the HP turbine, HP evaporator and condenser in descending order, respectively. In the same manner, in HP turbine the capital investment cost $\dot{Z}_{LP\_turb}$ value dominates the contribution associated with exergy destruction $\dot{C}_{D,HP\_turb}$.

This implies, lowering the value of $\dot{Z}+\dot{C}_D$ in the HP turbine would come by choosing turbine with lower capital investment cost.

Other components are observed to follow similar trend. The high value of f for these components indicates that the capital investment cost $\dot{Z}$, is larger than the cost rate associated with exergy destruction $\dot{C}_D$. Therefore, any further reduction in the value of $\dot{Z}+\dot{C}_D$ parameter can be achieved by lowering the capital investment cost of the components.

Comparing the processes involving compression in the pump, expansion in the turbines and heat transfer in the superheater, evaporators and preheaters, the LP pump1 and superheater are observed to have lower value of rate of exergy destruction $\dot{E}_D$ than other components in the DORC. The superheater and LP pump1 also appears to have lower value of $\dot{Z}+\dot{C}_D$ compare to other components of the cycle, in which superheater has the lowest value of $\dot{Z}+\dot{C}_D$, which is understandable considering the degree (1˚C) of superheating in the base case. Therefore, the LP pump1 and superheater are considered the cheapest components in the cycle with minimum values of $\dot{Z}+\dot{C}_D$ and having no significant effect on the exergoeconomic performance of the cycle given any changes in the component. It is also observed that all the components where heat transfer process occur except in the superheater, have high rate of exergy destruction $\dot{E}_D$ with corresponding high cost associated with exergy destruction $\dot{C}_D$.

5.2. Parametric Study

In this section, an investigation on the effect of operating parameters on the

cycle thermodynamic and exergoeconomic performance is undertaken. **Figure 2** shows the influence of HP and LP pressures variation on the DORC thermal efficiency and cycle power outputs. Analysis indicates that, as HP pressure increases while LP pressure is held constant, the power output of the HP turbine decreases.

Thermal efficiency: **Figure 2(a)** shows the variation of thermal efficiency (η_{th}) with respect to changes in P_{HP} and P_{LP} pressures. The η_{th} trend terns to gradually decrease as the value of P_{HP} rises and sharply increases with P_{LP} rise. This is because the increase in P_{LP} leads to a decrease in heat source utilization rate and increase in T_{19} temperature. That is, as P_{LP} increases heat absorbed in the HP evaporator $\dot{Q}_{HPE}$ decreases, heat absorbed in the LP evaporator $\dot{Q}_{LPE}$ decreases and heat absorbed in the LP preheater 1 $\dot{Q}_{preH1}$ increases at first and then decrease. Since the total amount of heat $\dot{Q}_{Total}$ absorbed by the

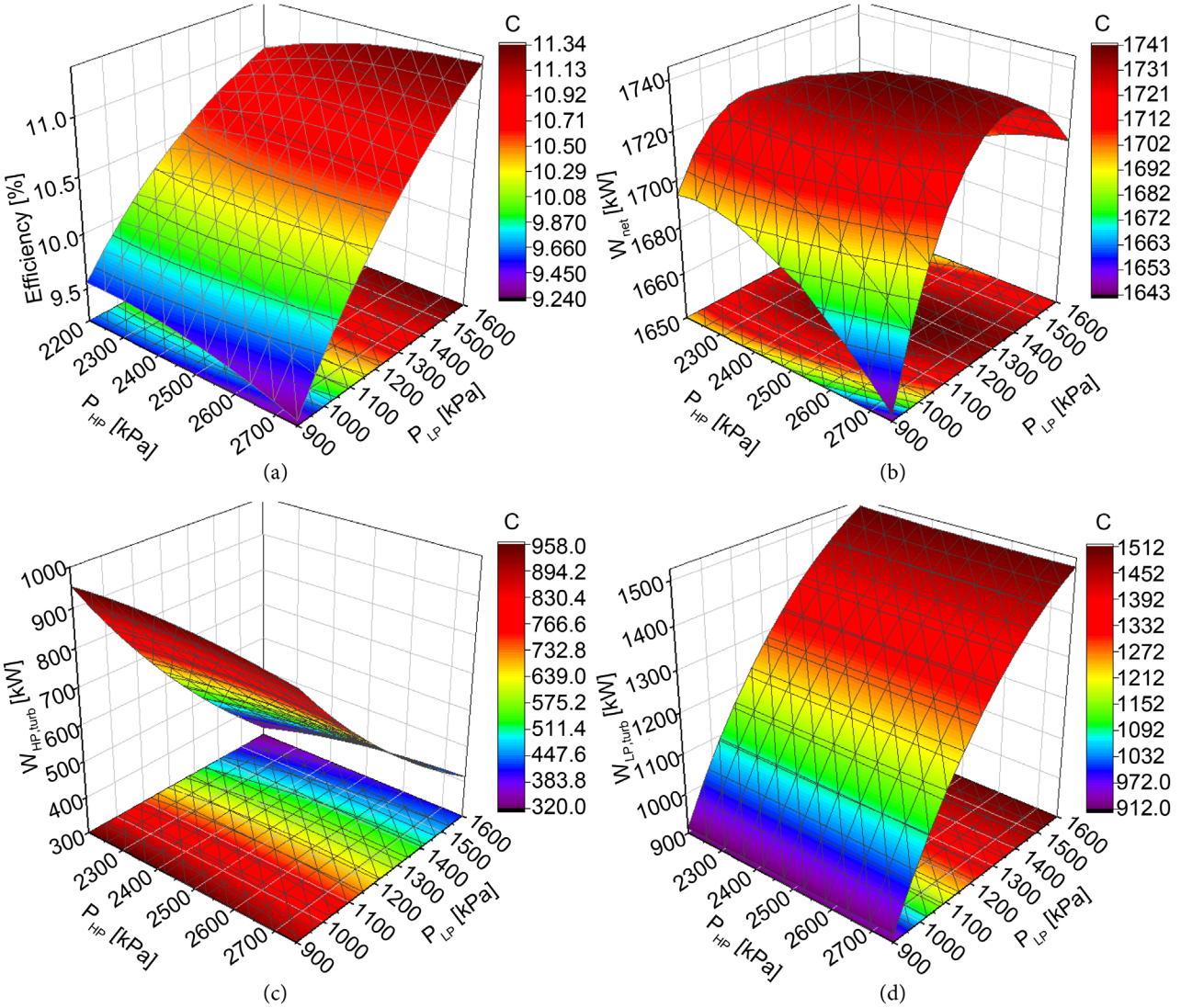

Figure 2. (a) Thermal efficiency (η_{th}) over P_{HP} and P_{LP} variation. (b) Net power output ($\dot{W}_{net}$) over P_{HP} and P_{LP} variation. (c) $\dot{W}_{HP\_turb}$ over P_{HP} and P_{LP} variation. (d) $\dot{W}_{LP\_turb}$ over P_{HP} and P_{LP} variation.

cycle is determined by $\dot{Q}_{HPE}$ and $\dot{Q}_{preH1}$, in which the value of $\dot{Q}_{HPE}$ dominants the value of $\dot{Q}_{Total}$, which decreases at first and then increases afterwards. Therefore, causing thermal efficiency η_{th} to increase as the value of P_{LP} increases. The highest η_{th} is observed within the range $2450\text{ kPa} < P_{HP} < 2750\text{ kPa}$ and $1400\text{ kPa} < P_{LP} < 1600\text{ kPa}$ (see **Figure 2(a)**).

Net power output: **Figure 2(b)** illustrates the effect of P_{HP} and P_{LP} pressure variation on the DORC system net power output. It can be observed, that when P_{HP} increases the value of $\dot{W}_{net}$ decreases, whereas the rise in P_{LP} causes $\dot{W}_{net}$ to increase at first and then declined afterward. This trend is due to the different responses of $\dot{W}_{HP\_turb}$ and $\dot{W}_{LP\_turb}$ to changes in P_{HP} and P_{LP}.

As P_{LP} increases while P_{HP} is held constant, the value of $\dot{W}_{HP\_turb}$ decreases (**Figure 2(c)**) while $\dot{W}_{LP\_turb}$ increases steadily (**Figure 2(d)**). Similarly, as P_{HP} increases while P_{LP} is constant, the value of $\dot{W}_{HP\_turb}$ decreases gradually while $\dot{W}_{LP\_turb}$ is reasonably unchanged. These effects lead to an initial increase in the value of $\dot{W}_{net}$ and a decline afterward as P_{LP} increases and a steady decline in $\dot{W}_{net}$ as P_{HP} increases. The higher value of $\dot{W}_{net}$ can be observed in the range of $1000\text{ kPa} < P_{LP} < 1500\text{ kPa}$ and $2300\text{ kPa} < P_{HP} < 2500\text{ kPa}$ as indicated in **Figure 2(b)**. η_{th} and $\dot{W}_{net}$ results presented show strong agreement with findings in [2].

Figure 3 shows variation in exergoeconomic parameters such as $\dot{C}_{D,overall}$, $\dot{Z}_{overall}$, $\dot{C}_{D,overall} + \dot{Z}_{overall}$, $f_{overall}$ and $c_{w,turb}$ over changes in the high-stage pressure (P_{HP}) and low-stage pressure (P_{LP}) of the cycle. **Table 7** indicates that the $\dot{Z} + \dot{C}_D$ value of the LP turbine, HP turbine and HP evaporator have the largest influence on the exergoeconomic performance of the cycle. If the value of P_{HP} is increased while P_{LP} is held constant, the values of $\dot{C}_{10}$, $\dot{C}_{11}$ and $\dot{C}_{D,LP\_turb}$ will have a slight decreasing trend while the LP turbine capital investment cost $\dot{Z}_{LP\_turb}$ remaining fairly constant. The values of $\dot{C}_8$ and $\dot{Z}_{HP\_turb}$ takes a descending trend and the value of $\dot{C}_{D,HP\_turb}$ is observed to slightly increase. The values of $\dot{C}_6$, $\dot{C}_7$, $\dot{Z}_{HP\_evap}$ and $\dot{C}_{D,HP\_evap}$ all takes a descending trend.

If the P_{LP} is increased while P_{HP} is kept constant, the values of $\dot{C}_{10}$, $\dot{C}_{11}$, $\dot{Z}_{LP\_turb}$ and $\dot{C}_{D,LP\_turb}$ showing similar trend, increasing steadily as P_{LP} increases. The value of $\dot{C}_8$ increases, the $\dot{Z}_{HP\_turb}$ show a declining trend, while the parameter $\dot{C}_{D,HP\_turb}$ ascend at first and then descend afterward. The $\dot{C}_6, \dot{C}_7$ and HP evaporator cost rate associate with exergy destruction $\dot{C}_{D,HP\_Evap}$ show slight increase and the parameter $\dot{Z}_{HP\_Evap}$ remains unchanged. It is obvious that changes in these component parameters can significantly influences the overall exergoeconomic performance of the DORC system.

In the case of P_{HP} increasing and P_{LP} constant, the $\dot{C}_D$ shows a descending trend for the LP turbine and HP evaporator and an increasing trend for HP turbine. These components account for up to half of the value of the overall cost rate associated with exergy destruction, $\dot{C}_{D,overall}$, therefore affecting the behavior of $\dot{C}_{D,overall}$. **Figure 3(a)** shows that the value of $\dot{C}_{D,overall}$ decreases as P_{HP}

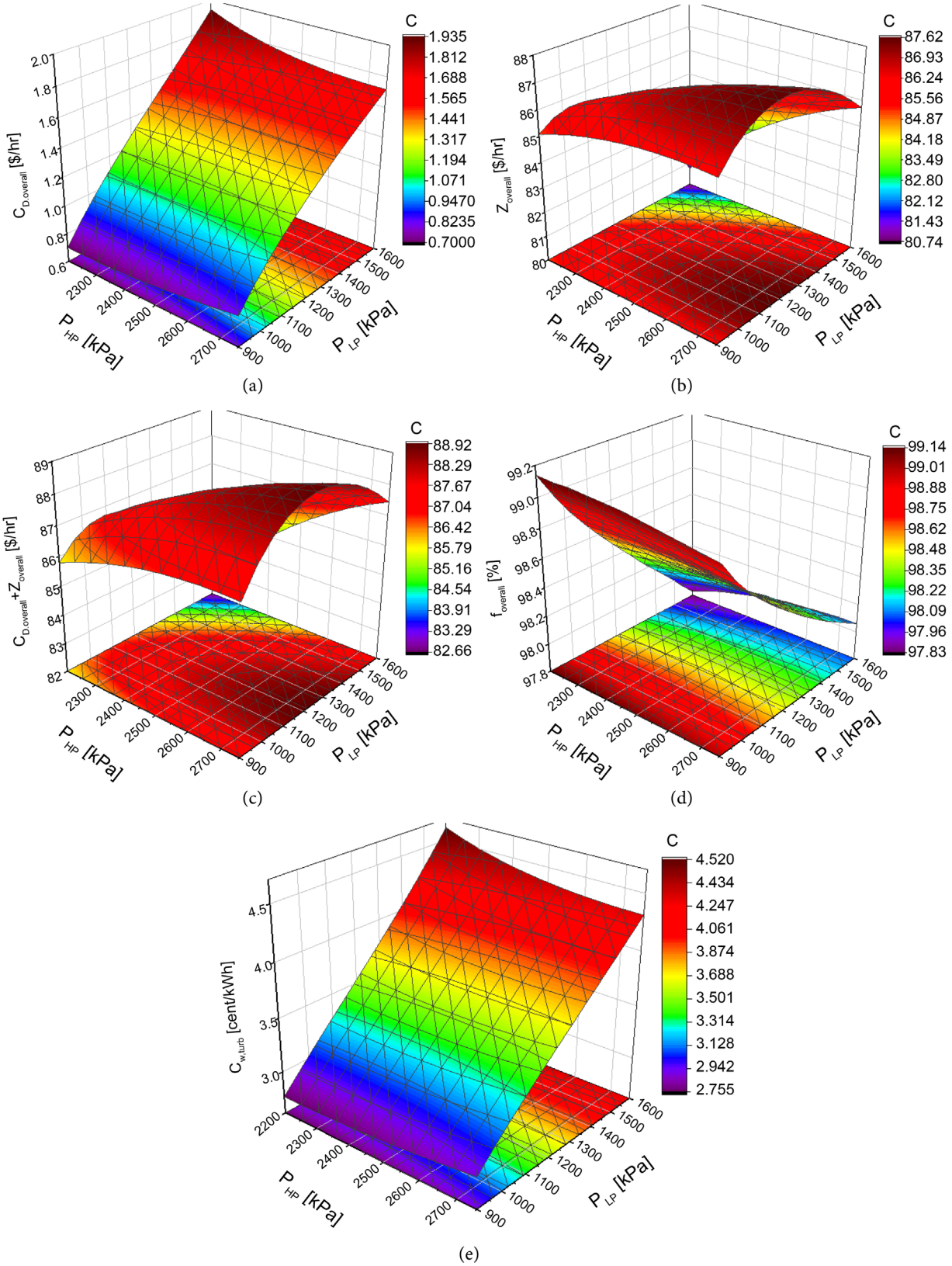

Figure 3. (a) $\dot{C}_{D,overall}$ over P_{HP} and P_{LP} variation. (b) $\dot{Z}_{overall}$ over P_{HP} and P_{LP} variation. (c) $\dot{C}_{D,overall}+\dot{Z}_{overall}$ over P_{HP} and P_{LP} variation. (d) $f_{overall}$ over P_{HP} and P_{LP} variation. (e) $c_{w,turb}$ over P_{HP} and P_{LP} variation.

is increased and P_{LP} is constant. This indicate that $\dot{C}_{D,LP\_turb}$, $\dot{C}_{D,HP\_evap}$ and other components with descending trend have stronger influence on the behavior of $\dot{C}_{D,overall}$. The $\dot{Z}_{overall}$ trend is observed to first increase and then decrease as P_{HP} is increased and P_{LP} held constant (**Figure 3(b)**). The trend of $\dot{Z}_{overall}$ can be attributed to the behavior of $\dot{Z}_{HP\_turb}$ and $\dot{Z}_{HP\_evap}$. Since the value $\dot{Z}_{overall}$ is greater than that of $\dot{C}_{D,overall}$, the $\dot{C}_{D,overall}+\dot{Z}_{overall}$ parameter have similar trend as the $\dot{Z}_{overall}$ parameter, ascending at first and then descending as P_{HP} increases (**Figure 3(c)**). The value of $f_{overall}$ parameter, which is the ratio of $\dot{Z}_{overall}$ and $\dot{C}_{D,overall}+\dot{Z}_{overall}$ show decreasing trend as P_{HP} increases. The unit cost of power produced $c_{w,turb}$ show slight decrease as P_{HP} increases.

If P_{LP} is increased and P_{HP} is held constant, the value of $\dot{C}_D$ for components with significant influence on the behavior of $\dot{C}_{D,overall}$ such as the LP turbine and HP evaporator show an increasing trend.

This results in the ascending trend of $\dot{C}_{D,overall}$ as P_{LP} increases. In the other hand, the $\dot{Z}_{overall}$ parameter have similar behavior as previous, increasing at first and then decreasing. $\dot{C}_{D,overall}+\dot{Z}_{overall}$ also takes a similar trend due to the dominant influence of $\dot{Z}$. The $f_{overall}$ parameter show increasing trend with increase in P_{LP}, reflecting the dominance of $\dot{Z}_{overall}$ in the $\dot{C}_{D,overall}+\dot{Z}_{overall}$ parameter.

5.3. Optimization

The DORC system optimization is considered in this section to determine the optimal design (working conditions) from the viewpoint of the exergy efficiency optimal design (EEOD), and the minimum unit cost of product cost optimal design (PCOD) using the direct search method in EES software. Six decision parameters with the range of variation shown below were considered to optimize the system:

$$2200\ \text{kPa} \le P_{HP} \le 2750\ \text{kPa}$$

$$900\ \text{kPa} \le P_{LP} \le 1600\ \text{kPa}$$

$$1^{\circ}\text{C} \le \Delta T_{SH} \le 10^{\circ}\text{C}$$

$$25^{\circ}\text{C} \le T_{cond,out} \le 29^{\circ}\text{C}$$

$$1^{\circ}\text{C} \le \Delta T_{cond,pp} \le 10^{\circ}\text{C}$$

$$5^{\circ}\text{C} \le \Delta T_{Evap,pp} \le 15^{\circ}\text{C}$$

The results of the optimization presented in **Table 8**, compares the performance of the base case, EEOD and PCOD cases. The exergy efficiency in the EEOD case is 33.03% which is 0.3% and 0.1% higher than the values obtained from the base cases and the PCOD case, respectively. The thermal efficiency in the EEOD case is 11.3%, which is 6.19% and 4.24% higher than the base case and PCOD, respectively. The net power produced in the EEOD case is 1939 kW, which is 10.2% higher than the base case and 2.24% lower than the PCOD case, respectively. With regards to the minimum unit cost product/power optimal

Table 8. Results of optimization.

Parameters	Optimization		
	Base case	EEOD	PCOD
P_{HP} [Pa]	2525	2481	2590
P_{LP} [Pa]	1250	1200	1059
ΔT_{SH} [C]	1	1	1
ΔT_{Evap_pp} [C]	10	10	5
ΔT_{cond_pp} [C]	10	5	6.66
η_{ex} [%]	32.93	33.03	33
η_{th} [%]	10.6	11.3	10.82
W_{net} [kW]	1741	1939	1991
$c_{w,turb}$	3.592	3.507	3.059
θ [%]	66.39	69.38	74.39
η_{sys} [%]	7.039	7.841	8.05
$\dot{m}_{cooling}$ [kg/s]	877.3	909.7	692.9
$\dot{m}_{HP}$ [kg/s]	28.87	29.43	33.56
$\dot{m}_{LP}$ [kg/s]	14.48	14.5	14.58

design (PCOD) case, the $c_{w,turb}$ parameteris 3.059 cent/kWh, which is 17.4% and 14.64% lower than the base case and EEOD case, respectively. The net power output in the PCOD case is 1991 kW, which is 12.55% and 2.6% higher than base case and the EEOD case, respectively. It is apparent from Table 8, that in PCOD case both unit cost of product and net power produced are higher compared to the base case and EEOD case.

In Table 9, comparative assessment of the base case, EEOD and PCOD cases from a thermoeconomic viewpoint is presented. The analysis identifies the optimal design and components with the highest exergy destruction rate and exergoeconomic factors for component optimization and system improvement. The base case is observed to have the highest value of $\dot{E}_{D,overall}$ (110.609 kW), which is 7.36% and 6.53% higher than the EEOD and PCOD cases, respectively. The condenser has the highest contribution to the cycle total rate of exergy destruction and the superheater having the minimum contribution for all three cases.

The HP evaporator, LP turbine and condenser are observed to have the highest value of cost rate associated with exergy destruction $\dot{C}_D$, and the HP turbine and superheater having the lowest value. The components in Table 9 are being arranged in descending order of their $\dot{Z}+\dot{C}_D$ value. Results indicate that the HP evaporator and LP turbine have the highest values, this means that focus will be place on these components in terms of optimization and modification for component improvement and cost effectiveness. The high value for exergoeconomic factor f observed, indicates that the capital investment costs $\dot{Z}$ for these components are larger than the contribution of the cost rate associated with exergy destruction in the $\dot{Z}+\dot{C}_D$ parameter. Therefore, to lower value of

Table 9. Results of exergoeconomic analysis for base case, EEOD and PCOD.

Components	Rate of exergy destruction $\dot{E}_{D,J}$ (KW)			Cost rate of exergy destruction $\dot{C}_{D,J}$ ($/hr)			Cost rate of Investment $\dot{Z}_J$ ($/hr)			$\dot{C}_{D,J}+\dot{Z}_J$ ($/hr)			Exergoeconomic factors f(%)		
	Base case	EEOD	PCOD	Base case	EEOD	PCOD	Base case	EEOD	PCOD	Base case	EEOD	PCOD	Base case	EEOD	PCOD
HP Evaporator	14.640	15.580	14.200	0.16440	0.17080	0.13400	8.240	8.273	10.230	8.404	8.444	10.360	98.04	97.98	98.71
LP Turbine	14.270	16.250	14.320	0.26730	0.30710	0.19280	22.250	23.550	22.250	22.520	23.860	22.440	98.81	98.71	99.14
Preheater 2	8.323	8.780	8.836	0.11000	011340	0.09258	7.208	7.260	10.270	7.318	7.373	10.360	98.50	98.46	99.11
HP Pump 2	1.884	1.928	2.567	0.02919	0.02927	0.03147	6.349	6.338	7.437	6.378	6.367	7.469	99.54	99.54	99.58
Preheater 1	12.590	14.370	7.501	0.18450	0.20600	0.08467	6.831	6.946	8.588	7.016	7.152	8.673	97.37	97.12	99.02
LP Evaporator	11.470	11.840	9.752	0.12020	0.12120	0.08335	6.024	5.976	7.036	6.144	6.098	7.120	98.04	98.01	98.83
HP Turbine	6.229	6.636	9.138	0.07441	0.07745	0.09285	14.940	15.470	18.400	15.010	15.540	18.500	99.50	99.50	99.50
LP Pump 1	1.637	1.700	1.478	0.03096	0.03242	0.02011	4.003	3.888	3.683	4.034	3.920	3.703	99.23	99.17	99.46
Superheater	0.456	0.469	0.520	0.00534	0.00536	0.00518	3.963	3.956	3.881	3.968	3.962	3.886	99.87	99.86	99.87
Condenser	39.110	24.910	35.070	0.32640	0.20960	0.25110	7.139	8.880	8.392	7.465	9.090	8.643	95.63	97.69	97.09
Total	110.609	102.463	103.382	1.313	1.273	0.988	86.950	90.530	100.20	88.260	91.810	101.20	98.45	98.61	99.03

$\dot{Z}+\dot{C}_D$, effort to select components with low capital investment cost and operating and maintenance cost might be employed.

6. Conclusions

This work investigates the thermodynamic, exergoeconomicand optimization of the dual-pressure organic Rankine cycle (DORC) for the utilization of medium temperature geothermal source for power production. Since several literatures [2] [11] have reported the advantages of DORC over the simple organic Rankine (SORC) in terms of first and second law thermodynamic performance, this study focuses on the exergoeconomic analysis and optimization of DORC to determine the exergy cost rates at each stream and obtain an optimized design for minimum product costs. This study is important considering the complex configuration of DORC and the potential high investment costs associated with it. The study conclusions reveals that the LP turbine have the highest value of $\dot{Z}+\dot{C}_D$, followed by HP turbine and HP evaporator, and from exergoeconomic viewpoint these components should receive more attention to achieve system improvement. The high values of the exergoeconomic factor, f, for these components indicate that the capital investment cost $\dot{Z}$ dominate the contribution of cost rate due to exergy destruction in the $\dot{Z}+\dot{C}_D$ parameter. Therefore, the use of cheaper components like HP evaporator, LP turbine and HP turbine will have remarkable improvement on the system cost effectiveness. Also, two optimization cases were performed on the DORC with regards to maximum exergy effi-

ciency optimized design (EEOD) and minimum product cost optimized design (PCOD). The PCOD case proved to be the best with respect to both units cost of power produced and net power produced, with product unit cost of 17.4% and 14.64% lower than base case and EEOD case, respectively, and a net power output of 12.55% and 2.6% higher than the base case and EEOD, respectively.

It is observed that the condenser have the highest rate of exergy destroyed, $\dot{E}_D$ compared to the other components, which is due to exergy lost to cooling water in the condenser. To minimize this loses in the condenser, hence improve system performance, further investigations may be performed on how to utilize some energy in the LP turbine exit stream for absorption cooling or domestic water heating before entering the condenser.

Acknowledgements

The authors acknowledge the support of Department of Mechanical Engineering, Faculty of Engineering, Cross River University of Technology, Calabar, Nigeria.

Conflicts of Interest

The authors declare no conflicts of interest regarding the publication of this paper.

References

[1] Yang, M.H. and Yeh, R.H. (2015) Economic Performances Optimization of the Transcritical Rankine Cycle Systems in Geothermal Application. *Energy Conversion and Management*, **95**, 20-31. https://doi.org/10.1016/j.enconman.2015.02.021

[2] Wang, M., Chen, Y., Liu, Q. and Zhao, Y. (2018) Thermodynamic and Thermo-Economic Analysis of Dual-Pressure and Single Pressure Evaporation Organic Rankine Cycles. *Energy Conversion and Management*, **177**, 718-736. https://doi.org/10.1016/j.enconman.2018.10.017

[3] Li, J., Ge, Z., Duan, Y., Yang, Z. and Liu, Q. (2018) Parametric Optimization and Thermodynamic Performance Comparison of Single-Pressure and Dual-Pressure Evaporation Organic Rankine Cycles. *Applied Energy*, **217**, 409-421. https://doi.org/10.1016/j.apenergy.2018.02.096

[4] Tchanche, B. F., Lambrinos, G., Frangoudakis, A. and Papadakis, G. (2011) Low-Grade Heat Conversion into Power Using Organic Rankine Cycles—A Review of Various Applications. *Renewable and Sustainable Energy Reviews*, **15**, 3963-3979. https://doi.org/10.1016/j.rser.2011.07.024

[5] Braimakis, K. and Karellas, S. (2018) Energetic Optimization of Regenerative Organic Rankine Cycle (ORC) Configurations. *Energy Conversion and Management*, **159**, 353-370. https://doi.org/10.1016/j.enconman.2017.12.093

[6] International Renewable Energy Agency (IRENA) (2017) Geothermal Power: Technology Brief (September). International Renewable Energy Agency, Abu Dhabi.

[7] Guzovi, Z., Rašković, P. and Blatarić, Z. (2014) The Comparison of a Basic and a Dual-Pressure ORC (Organic Rankine Cycle): Geothermal Power Plant Velika Ciglena Case Study. *Energy*, **76**, 175-186. https://doi.org/10.1016/j.energy.2014.06.005

[8] Ziviani, D., Beyene, A. and Venturini, M. (2014) Advances and Challenges in ORC Systems Modeling for Low Grade Thermal Energy Recovery. *Applied Energy*, **121**, 79-95. https://doi.org/10.1016/j.apenergy.2014.01.074

[9] Lecompte, S., Huisseune, H., Van Den Broek, M., Vanslambrouck, B. and De Paepe, M. (2015) Review of Organic Rankine Cycle (ORC) Architectures for Waste Heat Recovery. *Renewable and Sustainable Energy Reviews*, **47**, 448-461. https://doi.org/10.1016/j.rser.2015.03.089

[10] Li, T., Zhang, Z., Lu, J., Yang, J. and Hu, Y. (2015) Two-Stage Evaporation Strategy to Improve System Performance for Organic Rankine Cycle. *Applied Energy*, **150**, 323-334. https://doi.org/10.1016/j.apenergy.2015.04.016

[11] Shokati, N., Ranjbar, F. and Yari, M. (2015) Exergoeconomic Analysis and Optimization of Basic, Dual-Pressure and Dual-Fluid ORCs and Kalina Geothermal Power Plants : A Comparative Study. *Renewable Energy*, **83**, 527-542. https://doi.org/10.1016/j.renene.2015.04.069

[12] Thierry, D.M., Flores-Tlacuahuac, A. and Grossmann, I.E. (2016) Simultaneous Optimal Design of Multi-Stage Organic Rankine Cycles and Working Fluid Mixtures for Low-Temperature Heat Sources. *Computers and Chemical Engineering*, **89**, 106-126. https://doi.org/10.1016/j.compchemeng.2016.03.005

[13] Manente, G., Lazzaretto, A. and Bonamico, E. (2017) Design Guidelines for the Choice between Single and Dual Pressure Layouts in Organic Rankine Cycle (ORC) Systems. *Energy*, **123**, 413-431. https://doi.org/10.1016/j.energy.2017.01.151

[14] Sadeghi, M., Nemati, A. and Yari, M. (2016) Thermodynamic Analysis and Multi-Objective Optimization of Various ORC (Organic Rankine Cycle) Configurations Using Zeotropic Mixtures. *Energy*, **109**, 791-802. https://doi.org/10.1016/j.energy.2016.05.022

[15] Li, J., Ge, Z., Liu, Q., Duan, Y. and Yang, Z. (2018) 'Thermo-Economic Performance Analyses and Comparison of Two Turbine Layouts for Organic Rankine Cycles with Dual-Pressure Evaporation. *Energy Conversion and Management*, **164**, 603-614. https://doi.org/10.1016/j.enconman.2018.03.029

[16] Klein, S.A. (2020) Engineering Equation Solver. F-Chart Software, Madison.

[17] Bejan, A., Tsatsaronis, G. and Moran, M. (1996) Thermal Design & Optimization. John Wiley & Sons Inc., New York.

[18] Ahmadzadeh, A., Reza, M. and Sedaghat, A. (2017) Thermal and Exergoeconomic Analysis of a Novel Solar Driven Combined Power and Ejector Refrigeration (CPER) System. *International Journal of Refrigeration*, **83**, 143-156. https://doi.org/10.1016/j.ijrefrig.2017.07.015

[19] Manente, G., Lazzaretto, A. and Bonamico, E. (2017) Design Guidelines for the Choice between Single and Dual Pressure Layouts in Organic Rankine Cycle (ORC) Systems. *Energy*, **123**, 413-431. https://doi.org/10.1016/j.energy.2017.01.151

[20] Kazemi, N. and Samadi, F. (2016) Thermodynamic, Economic and Thermo-Economic Optimization of a New Proposed Organic Rankine Cycle for Energy Production from Geothermal Resources. *Energy Conversion and Management*, **121**, 391-401. https://doi.org/10.1016/j.enconman.2016.05.046

[21] Cayer, E., Galanis, N. and Nesreddine, H. (2010) Parametric Study and Optimization of a Transcritical Power Cycle Using a Low Temperature Source. *Applied Energy*, **87**, 1346-1357. https://doi.org/10.1016/j.apenergy.2009.08.031

Appendix A: Equipment Cost ($\dot{Z}_J$) Calculation

The equations for calculating the equipment purchase cost for the turbine, pumps and heat exchangers are expressed as follows [1] [21]:

$$Z_{turb} = C_{P,turb}\left(F_{M,turb}F_{P,turb}\right) \tag{A.1}$$

$$Z_{pump} = C_{P,pump}\left(B_{1,pump} + B_{2,pump}F_{M,pump}F_{P,pump}\right) \tag{A.2}$$

$$Z_{HX} = C_{P,HX}\left(B_{1,HX} + B_{2,HX}F_{M,HX}F_{P,HX}\right) \tag{A.3}$$

where C_P refers to component bare module cost and can be calculated as follows:

$$\log C_{P,x} = K_{1,x} + K_{2,x}\log Y + K_{3,x}\left(\log Y^2\right) \tag{A.4}$$

where Y in Equation (A.4) indicates the capacity of the turbine and pump, or the area in the case of the heat exchanger. K_1, K_2 and K_3 are coefficients of equipment cost given in **Table A1**. F_M is the material factor, and B_1 and B_2 are constants given in **Table A1**. F_P is the pressure factor and can be obtained as follows:

$$\log F_{P,x} = C_{1,x} + C_{2,x}\log\left(10P-1\right) + C_{3,x}\left(\log\left(10P-1\right)\right)^2 \tag{A.5}$$

C_1, C_2 and C_3 are constants given in **Table A1**. The Marshall and Swift equipment cost indices [21] is utilized to convert Equations (A.1)-(A.3) from reference year to present year (2021).

$$C^*_{2021} = C_{original\ cost}\frac{CI^{2021}_{M.S}}{CI^{reference\ year}_{M.S}} \tag{A.6}$$

The LMTD method has been adopted in the present study to calculate the heat exchange area. The heat transfer rate in heat exchanger can be expressed as [1]:

$$Q = U_k A_k \Delta T_{mean} \tag{A.7}$$

Table A1. Equipment cost parameters [21].

X	Y	K_1	K_2	K_3	B_1	B_2	C_1	C_2	C_3	F_M
Turbine	$\dot{W}_{turb}$	2.2476	1.4965	−0.1618	0	1	0	0	0	3.4
Pump	$\dot{W}_{pump}$	3.3892	0.0536	0.1538	1.89	1.35	−0.3935	0.3957	−0.0023	1.6
Heat exchanger	A_{HX}	4.3247	−0.3030	0.1634	1.63	1.66	0.0388	−0.1127	0.0818	1

Table A2. Approximate values of overall heat transfer coefficient from several heat exchangers.

Components	Overall heat transfer coefficient, U_k (kW/(m^2 K))
Evaporator	0.9
Condenser	1.1
Heat exchanger	1.0

where ΔT_{mean} is the logarithmic mean temperature difference between the working fluid and the coolant, and U_k is the overall heat transfer coefficient given in Table A2.